

Single-particle versus collective effects in assemblies of nanomagnets: screening

F. Vernay and H. Kachkachi

*Université de Perpignan Via Domitia, Laboratoire PROMES-CNRS (UPR-8521),
Rambla de la Thermodynamique, Tecnosud, 66100 Perpignan, FRANCE.*

(Dated: July 8, 2019)

We discuss experimentally realizable situations in which surface effects may “screen out” the dipolar interactions in an assembly of nanomagnets, which then behaves as a noninteracting system. We consider three examples of physical observables, equilibrium magnetization, ac susceptibility and ferromagnetic resonance spectrum, to illustrate this screening effect. For this purpose, we summarize the formalism that accounts for both the intrinsic features of the nanomagnets and their collective effects within an assembly the condition for screening.

I. INTRODUCTION

For many years research on assemblies of nanomagnets (NM) has been devoted to the investigation of the two aspects: i) the single-nanomagnet (SNM) physics that is mostly governed by the finite size and boundary effects which become rather acute at the nanometer scale, ii) the collective behavior of the assembly (ANM) that is mostly driven by the mutual long-range dipolar interactions. Numerous studies, experimental and theoretical, have been carried out in order to investigate the interplay between the phenomena that occur at these two rather different scales: While the relevant temperature at the SNM scale is about a few degrees (Kelvin), it is about a few tens of degrees for the ANM. While the relevant relaxation time is about a nanosecond for the former, it is about a few minutes or hours for the latter, and so on.

From the technological perspective, many challenging issues are still open. For example, to what extent assembling into macro-scaled systems and devices various kinds of nano-objects may preserve their novel properties pertaining to the nanoscale? From a fundamental viewpoint, the foremost aim is to achieve a clear understanding of the behavior of the nano-scaled systems and this requires the development of new and adequate tools for their probe, measurement and modeling. Indeed, the transition from the nano-scale to the macro-scale requires a fair understanding of the interplay between the intrinsic properties of the nano-objects, taken separately, and their mutual interactions when they are assembled into more complex structures. An example of paramount importance for practical applications is concerned with the dynamics of the assembly and how it is related to the SNM dynamics. This issue has been investigated for decades and the debate is still at its climax, for instance in what regards the conditions under which a spin-glass behavior or a superferromagnetic order may be observed, for a given set of physical parameters of the individual NM.

Conversely, one may address the question as to whether it is possible to define a set of such SNM parameters, on one hand, and those pertaining to the ANM, on the other, so that somehow the ANM would behave

as a free assembly of “dressed” NM. In other terms, the intrinsic properties of the individual NM, such as surface effects (SE), would screen out the dipolar interactions (DI) within the assembly. For example, it has been shown by many researchers [1, 2] that one can control the inter-particle interactions by tuning the properties of the NM themselves. On the other hand, it is possible to modify the NM properties by modifying the assembly characteristics (shape, spatial organization, etc) [3, 4].

In the present work, we contribute to this study by establishing the conditions, realizable in experiments, under which the above-mentioned screening may occur. For this, we first summarize our previous work that has been carried out with the objective to build a global picture that encompasses both what is happening at the SNM and at the assembly level. Indeed, we have built a complete theoretical toolbox for dealing with the collective behavior of an ANM while taking account of the NM features.

The paper is organized as follows: in Section II we summarize our formalism for the single SNM and the corresponding effective model that accounts for the intrinsic properties such as SE. In Section III we discuss the DI in a formalism that takes account of the finite-size of the NM and is compared to the point-dipole approximation. In Section IV we consider in three successive paragraphs the equilibrium magnetization, the ac susceptibility and the ferromagnetic resonance spectrum. In each case we discuss the screening of the DI by the SE and establish, when analytically possible, the corresponding conditions. The final section is devoted to conclusions and discussion.

II. SINGLE NANOMAGNET

For the single NM considered as a crystallite of \mathcal{N} atomic magnetic moments $\mathbf{m}_i = m\mathbf{s}_i$ ($\|\mathbf{s}_i\| = 1$), it is possible in principle to investigate, to some extent, most of the magnetic properties (at equilibrium and out-of-equilibrium)[5–12]. This is usually done with the help of the atomistic approach based on the anisotropic (classical) Heisenberg Hamiltonian

$$\mathcal{H} = -\frac{1}{2} \sum_{i,j} J_{ij} \mathbf{s}_i \cdot \mathbf{s}_j - \mu_a \mathbf{H} \cdot \sum_{i=1}^{\mathcal{N}} \mathbf{s}_i - \sum_{i=1}^{\mathcal{N}} K_i \mathcal{A}(\mathbf{s}_i) \quad (1)$$

with the usual meaning for the microscopic parameters J, K . $\mathcal{A}(\mathbf{s}_i)$ is the anisotropy function that depends on the locus of the atomic spin \mathbf{s}_i . So for core spins, the anisotropy may be uniaxial and/or cubic, while for surface spins there are various models for on-site anisotropy that is very often taken as uniaxial with either a transverse or parallel easy axis. There is also the more plausible model of Néel for which $\mathcal{A}(\mathbf{s}_i) = \frac{1}{2} \sum_{j=1}^{z_i} (\mathbf{s}_i \cdot \mathbf{u}_{ij})^2$, where z_i is the coordination number at site i and \mathbf{u}_{ij} a unit vector connecting the nearest neighbors i, j . The constant $K_i > 0$ is usually denoted by K_c if the site i is in the core and by K_s if it is on the boundary.

However, it is a very difficult, if not impossible, task to deal with the dynamics, especially the calculation of the relaxation rate and magnetization reversal. Indeed, it is a formidable task to perform a detailed analysis of the various critical points (minima, maxima, saddle points) of the energy which is required for the study of the relaxation processes.

In fact, it has been shown that, under some conditions which are quite plausible for today's state-of-the-art grown nanomagnets, namely of weak surface disorder, one can map this atomistic approach onto a macroscopic model for the net magnetic moment

$$\mathbf{m}_i = \frac{1}{\mathcal{N}} \sum_{i=1}^{\mathcal{N}} \mathbf{s}_i \quad (2)$$

of the NM evolving in the effective potential (H.O.T. = higher-order terms)

$$\mathcal{E}_{\text{eff}} = -K_2 m_z^2 + K_4 (m_x^4 + m_y^4 + m_z^4) + \text{H.O.T.} \quad (3)$$

In the sequel we will refer to Eqs. (3, 2) as the effective-one-spin problem (EOSP).

The leading terms have coefficients K_2 and K_4 that are functions of the atomistic parameters (J, K_c, K_s, z , etc) and of the size and shape of the NM [13–15]. Note that both the core and surface may contribute to K_2 and K_4 . For example, when the anisotropy in the core in Eq. (1) is uniaxial, $K_2 \simeq K_c N_c / \mathcal{N}$, where N_c is the number of atoms in the core, see Ref. 16. In fact, even in this case the quartic term appears and is a pure surface contribution. Regarding the coefficient of the quartic contribution ($k \equiv K/J$), for a sphere we have $k_4 = \kappa k_s^2 / zJ$ where κ is a surface integral [13] and for a cube $k_4 = (1 - 0.7/\mathcal{N}^{1/3})^4 k_s^2 / zJ$ [15].

The most relevant parameter of this effective model is the ratio

$$\zeta \equiv K_4 / K_2 \quad (4)$$

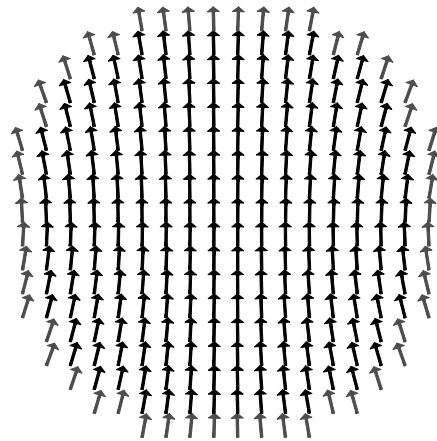


Figure 1: Spin structure of linear dimension $N = 20$.

which roughly represents the relative contribution of the surface disorder and the ensuing spin noncollinearities. The details of the conditions under which this model is applicable are discussed in Ref. 13 and may be summarized as follows. In order to plot the energy of a many-spin NM we introduce a Lagrange parameter which constrains the net magnetic moment to follow a specified path in its phase space spanned by the spherical coordinates (θ, φ) . For this to be applicable the spin misalignment (or canting) should not too strong. Therefore, the effective model can be built for NM whose SA, as compared to the spin-spin exchange coupling, is not too strong. On the other hand, the NM should not be too large for it to be considered as a single magnetic domain, for a given underlying material.

To sum up, we have at hand a macroscopic model whose dynamics can be studied using the full-fledged theory of Brown (or Langer) developed during the last decades by many authors. This is nothing new. But the new thing about this EOSP model is that it captures the main intrinsic features of the NM through the coefficients of its effective potential energy (3). In particular, we can investigate the effect of surface anisotropy on the relaxation rate of an individual NM. This was done in Ref. 17. Indeed, in Fig. 2 of this reference, the relaxation rate Γ is plotted against the parameter ζ , as computed analytically using Langer's (and Brown's) theory and numerically using the continued fraction method. Γ first increases as ζ increases, since in this case the quartic term in Eq. (3) creates saddle points at the equator, but the minima are still determined by the uniaxial anisotropy (the quadratic term). Beyond a critical value of ζ the energy landscape becomes that of a cubic anisotropy, namely the uniaxial-anisotropy minima become maxima and the new minima are at the diagonals $(\pm 1/\sqrt{3}, \pm 1/\sqrt{3}, \pm 1/\sqrt{3})$. As ζ further increases these minima become deeper and the energy barrier higher, thus leading to a decrease of Γ . A measurable observable that can be built out of Γ is the switching field (SF), *i.e.*

the field at which the magnetization of the NM switches at a given temperature and a given direction of the external magnetic field. Upon varying the orientation of the latter, we obtain the so-called Stoner-Wohlfarth astroid or the curve of the limit of metastability. The measurement and discussion of the various aspects of the SF in various situations of anisotropy can be found in the review 18. Experimental observation of the magnetization reversal depends on the relaxation time of the cluster and on the measuring time τ_m of the experimental setup. The magnetization reversal can be observed only if the relaxation time is in the time window of the experiment, or equivalently, if the relaxation rate is equal to the measuring frequency $\nu_m = \tau_m^{-1}$. Therefore, for the experimental observation of the magnetization reversal at finite temperature, the relaxation rate as a function of the reduced anisotropy barrier [36]

$$\sigma = KV/k_B T, \quad (5)$$

ζ , the SF h_s , the angle ψ between the applied field and the anisotropy axis and the damping parameter α , must be equal to the measuring frequency ν_m , *i.e.*

$$\Gamma(\sigma, \zeta, h_s, \psi, \alpha) = \nu_m. \quad (6)$$

This equation can then be (numerically) solved for h_s in terms of $\nu_m, \sigma, \zeta, \alpha$ and ψ . Obviously, at very low temperature and $\zeta = 0$ this yields the SW astroid with the main feature that it homothetically shrinks as the temperature increases and reaches zero at the blocking temperature. This was confirmed by experiments on single cobalt NM using the microSQUID technique [19].

For finite values of ζ one can also build the parametric plot of the two components of the SF, namely $h_x = h_s \sin \psi, h_z = h_s \cos \psi$. The result is given in Fig. 2 of Ref. 17. The new feature that this plot shows is that the effect of finite ζ (*i.e.* that of surface anisotropy) is a flattening of the astroid along one direction. For an experimental confirmation of such a flattening of the SF curves, see the results in Fig. 6 of Ref. 3 obtained for 8 nm maghemite NM. We note that this flattening of the SF curve owing to SA was observed in Refs. 10, 20, where such a curve was computed at very low temperature, using the model in Eq. (1), for a spherical many-spin particle with local (on-site) anisotropy, uniaxial in the core and transverse on the surface with a variable constant.

III. ASSEMBLY OF FINITE-SIZE NANOMAGNETS

Here we briefly discuss another important extension that is relevant to an interacting ANM of given size and shape. More precisely, we would like to emphasize that, when dealing with DI between NM, even in the macrospin

approximation (ignoring SE), one has to take account of their size and shape. Ignoring these parameters is what is done in the so-called point-dipole approximation (PDA) which is rather poor and may even lead to wrong results in situations with NM too close to each other. Think of two magnetic layers that are infinitely close to each other, for which the PDA predicts a finite dipolar coupling energy while in reality the dipolar coupling between the planes goes to zero, see Refs. 21, 22.

In brief, for two finite-size elements, say of cylindrical symmetry and of diameter $2R$ and thickness $2t$ with a center-to-center distance d , one subdivides them into (differential) magnetic elements $d\mathbf{m}_i, i = 1, 2$, assumed to be point dipoles, and then writes the energy of their DI as follows

$$d\mathcal{E}_{\text{DI}} = \left(\frac{\mu_0}{4\pi}\right) \frac{d\mathbf{m}_1 \cdot d\mathbf{m}_2 - 3(d\mathbf{m}_1 \cdot \mathbf{e}_{12})(d\mathbf{m}_2 \cdot \mathbf{e}_{12})}{r_{12}^3}.$$

For any two such NM within the assembly we write

$$d\mathcal{E}_{\text{DI}}^{(i,j)} = -\left(\frac{\mu_0}{4\pi}\right) d\mathbf{m}_i \cdot \mathcal{D}_{ij} d\mathbf{m}_j$$

where \mathcal{D}_{ij} is the DI tensor

$$\mathcal{D}_{ij} \equiv \frac{1}{r_{ij}^3} (3\mathbf{e}_{ij}\mathbf{e}_{ij} - 1), \quad \mathbf{r}_{ij} = \mathbf{r}_i - \mathbf{r}_j, \quad \mathbf{e}_{ij} = \frac{\mathbf{r}_{ij}}{r_{ij}}. \quad (7)$$

The next step consists in integrating over the whole volume of each NM leading to the DI energy [22]

$$\mathcal{E}_{\text{DI}} = \eta [\mathbf{s}_1 \cdot J_{12} \mathbf{s}_2 - 3\psi_{12} (\mathbf{s}_1 \cdot \mathbf{e}_{12})(\mathbf{s}_2 \cdot \mathbf{e}_{12})] \quad (8)$$

where the (diagonal) matrix J_{12} and the coefficient ψ_{12} are given by

$$\begin{cases} J_{12} = I, & \psi_{12} = 1, & \text{vertical setup,} \\ J_{12} = \begin{pmatrix} 1 & 0 & 0 \\ 0 & 1 & 0 \\ 0 & 0 & \Phi_{12} \end{pmatrix}, & \psi_{12} = \frac{2+\Phi_{12}}{3}, & \text{horizontal setup,} \end{cases} \quad (9)$$

and λ is the (dimensionless) coupling constant

$$\eta = \left(\frac{\mu_0}{4\pi}\right) \frac{(M_s V)^2 / d^3}{KV} \times \begin{cases} \mathcal{I}_s^v(\varrho\tau), & \text{vertical planes,} \\ \mathcal{I}_d^v(\varrho, \tau), & \text{vertical disks,} \\ \mathcal{I}_d^h(\varrho, \tau) & \text{horizontal disks.} \end{cases} \quad (10)$$

and

$$\varrho \equiv \frac{d}{2t}, \quad \tau \equiv \frac{t}{R}.$$

For later reference, we introduce the DI parameter λ

$$\lambda \equiv \left(\frac{\mu_0}{4\pi}\right) \frac{(M_s V)^2 / d^3}{KV}. \quad (11)$$

Finally, $\Phi_{12}(\varrho, \tau) \equiv \mathcal{I}_d^h(\varrho, \tau) / \mathcal{I}_d^h(\varrho, \tau)$. $\mathcal{I}_d^h(\varrho, \tau)$ and $\mathcal{J}_d^h(\varrho, \tau)$ are two shape integrals given explicitly by Beggiola *et al.* [23]

Note that the dipolar energy (8) depends, on one hand, on the size and shape of the NM and on the other, on their spatial arrangement via the parameters ρ, τ , and ξ . For example, the integral \mathcal{I}_s^v that obtains for two vertically stacked planes, of lateral dimension L and a distance d apart, reads ($\delta \equiv d/L$) [21, 22]

$$\mathcal{I}_s^v(\delta) = 4\delta^3 \left[\begin{array}{c} \delta - 2\sqrt{1+\delta^2} + \sqrt{2+\delta^2} \\ + \frac{1}{2} \log\left(1 + \frac{1}{\delta^2}\right) + \log\left(\frac{1+\sqrt{1+\delta^2}}{1+\sqrt{2+\delta^2}}\right) \end{array} \right].$$

For small values of δ the integral $\mathcal{I}_s^v(\delta)$ increases with δ as $4\delta^3 \left[\sqrt{2} - 2 + \log\left(\frac{2}{\delta(1+\sqrt{2})}\right) \right]$ while for large δ it does so as $1 - \delta^{-2} + 17\delta^{-4}/16$. We thus see that as the distance between the two magnetic layers becomes very small, *i.e.* $\delta \rightarrow 0$, the integral $\mathcal{I}_s^v(\delta)$ and thereby the DI vanishes as it should. This result cannot be obtained within the PDA for which J_{12} and ψ_{12} in Eq. (8) are equal to unity. On the other hand, as the two magnets are very far apart, *i.e.* δ becomes very large, $\mathcal{I}_s^v(\delta) \rightarrow 1$ and thereby the DI reaches the limit of the PDA.

IV. SINGLE NM VERSUS ASSEMBLY

We have now presented the two ingredients that are necessary for studying the competition between the SNM features and the collective behavior in an array of NM. We have chosen to do so through three observables, namely the equilibrium magnetization as a function of the external magnetic field, the ac susceptibility and the FMR spectrum.

A. Equilibrium magnetization

Here we discuss some old experimental results regarding the behavior of the magnetization of ANM as a function of the applied magnetic field at varying temperature. This is our first example of compensation between SE and DI.

Measurements of the magnetization at high fields performed on the γ -Fe₂O₃ nanoparticles [4, 24] and on cobalt particles [25] showed that the magnetization is strongly influenced by surface effects, as was evidenced by the experimental study with variable particle size, see Fig. 3 of Ref. [4] and by (Monte Carlo) numerical investigation of Ref. [26]. One finds that the $M(H)$ curves at different temperatures present a rather different behavior as we compare dilute with concentrated assemblies. Indeed, in Ref. 4 (Fig. 3) the $M(H)$ curves look regular from

300 K down to 100 K, split below 100 K and instead of saturating, the magnetization increases with increasing field and decreasing temperature. The low-temperature increase starts at 100 – 75 K and becomes steeper as the temperature decreases. This steep increase is less important with the increasing particle size, in accordance with the study of SE in Ref. 26. A similar behavior is observed with increasing concentration. For more concentrated dispersions the low-temperature effect is still present but less marked, compared to the corresponding dilute samples.

This interplay between surface anisotropy (an effect that is intrinsic to the NM) and the DI (an effect pertaining to the assembly) was studied in Refs. 27, 28, using both Monte Carlo simulations and analytical developments for dilute assemblies.

In Ref. 29 this was performed for an assembly of \mathcal{N} ferromagnetic NM each carrying a magnetic moment $\mathbf{m}_i = m_i \mathbf{s}_i$, $i = 1, \dots, \mathcal{N}$ of magnitude m_i and direction \mathbf{s}_i , with $|\mathbf{s}_i| = 1$. \mathbf{m}_i was defined in terms of the Bohr magneton μ_B , *i.e.* $m_i = n_i \mu_B$, and n_i are either all equal for monodisperse assemblies or chosen according to some distribution. Then, it was shown that in a dilute assembly, the magnetization of a NM at site i in a magnetic field applied in the z direction, to first order in the DI parameter, reads

$$\langle s_i^z \rangle \simeq \langle s_i^z \rangle_0 + \sum_{k=1}^{\mathcal{N}} \xi_{ik} \langle s_k^z \rangle_0 A_{ki} \frac{\partial \langle s_i^z \rangle_0}{\partial x_i}, \quad (12)$$

where $A_{kl} = \mathbf{e}_h \cdot \mathcal{D}_{kl} \cdot \mathbf{e}_h$. In Eq. (12) $\langle \cdot \rangle$ is the statistical average of the projection on the field direction of the particle's magnetic moment. The following useful dimensionless physical parameters are introduced

$$\xi_{ik} = \frac{\mu_0}{4\pi} \frac{m_i m_k / d^3}{k_B T}, \quad x_i \equiv \frac{n_i \mu_B H}{k_B T} = n_i x, \quad \sigma_i \equiv \frac{KV_i}{k_B T}.$$

It is worth emphasizing that Eq. (12) yields the (local) magnetization $\langle s_i^z \rangle$ of an interacting assembly in terms of its “free” (with no DI) magnetization $\langle s_i^z \rangle_0$ and susceptibility $\partial \langle s_i^z \rangle_0 / \partial x_i$, with of course the contribution of the assembly “superlattice” via the lattice sum. As such, in order to investigate the competition between DI and SE for example, one has to use for the SNM an expression for the magnetization $\langle s_i^z \rangle_0$ that takes account of SE. Restricting ourselves to monodisperse assemblies so as to investigate the interplay between intrinsic and collective effects in pure form. Then, $x_i = x$, $\sigma_i = \sigma$, $\xi_{ij} = \xi = \lambda \sigma$ [see Eq. (11)] and Eq. (12) simplifies into

$$\langle s^z \rangle \simeq m^{(0)} \left[1 + \xi \mathcal{C}^{(0,0)} \frac{\partial m^{(0)}}{\partial x} \right]. \quad (13)$$

The lattice sum $\mathcal{C}^{(0,0)}$ is the first of the hierarchy of lattice sums (see Ref. [29]). For large samples, we have

$\mathcal{C}^{(0,0)} = -4\pi(D_z - 1/3)$, where D_z is the demagnetizing factor in the z direction. It turns out that the relevant DI parameter, to this order of approximation, is in fact

$$\tilde{\xi} \equiv \xi \mathcal{C}^{(0,0)} = \xi \times \frac{1}{\mathcal{N}} \sum_{i,j=1, i \neq j}^{\mathcal{N}} A_{ij}.$$

The longitudinal susceptibility $\chi_{\parallel}^{(0)} = \partial m^{(0)}/\partial x$ is given in Ref. [30] and, injected in Eq. (13) leads to the approximate expression for the magnetization of a particle taking account of its DI with the other particles in the assembly

$$\langle s^z \rangle \simeq m^{(0)} \left[1 + \tilde{\xi} \left(a_0^{(1)} - \left(m^{(0)} \right)^2 \right) \right]. \quad (14)$$

Where $a_0^{(1)}$ can be computed in the high-energy barrier limit $a_0^{(1)} (\sigma \gg 1) \simeq 1 - \frac{1}{\sigma}$.

Note that in the absence of any interactions or anisotropy, or at high temperature, the magnetization is given by the Langevin function

$$\langle s^z \rangle_0 (\sigma \rightarrow 0, \xi \rightarrow 0) = \mathcal{L} \left(\frac{\mu_0 H M_S}{k_B T} \right). \quad (15)$$

Now, using the EOSP model (3) for the individual NM we compute the magnetization $m^{(0)}$ using perturbation theory for small $\zeta = K_4/K_2$, see Ref. 28 for the detailed derivation.

At first order in $\tilde{\xi}$, the equilibrium susceptibility reads

$$\chi^{\text{eq}}(x, \sigma, \zeta, \tilde{\xi}) \simeq \chi_{\text{free}}^{\text{eq}} + \tilde{\xi} \chi_{\text{int}}^{\text{eq}} \quad (16)$$

where $\chi_{\text{free}}^{\text{eq}}$ is linear susceptibility of the non-interacting assembly in the limit of high anisotropy energy barrier [28, 31]

$$\chi_{\text{free}}^{\text{eq}}(x, \sigma, \zeta) = 2\chi_0^{\perp} \sigma \left[\chi_{\text{free}}^{(1)} + 3\chi_{\text{free}}^{(3)} x^2 \right], \quad (17)$$

$$\begin{aligned} \chi_{\text{free}}^{(1)} &= \left(1 - \frac{1}{\sigma} \right) + \frac{\zeta}{\sigma} \left(-1 + \frac{2}{\sigma} \right), \\ \chi_{\text{free}}^{(3)} &= \frac{1}{3} \left[\left(-1 + \frac{2}{\sigma} \right) + \frac{\zeta}{\sigma} \left(2 - \frac{5}{\sigma} \right) \right]. \end{aligned}$$

Here χ_0^{\perp} is the transverse equilibrium susceptibility per spin at zero temperature in the absence of a bias field

$$\chi_0^{\perp} \equiv \left(\frac{\mu_0 m^2}{2KV} \right).$$

The contribution of DI to the equilibrium susceptibility

is given by [28]

$$\chi_{\text{int}}^{\text{eq}}(x, \sigma, \zeta) = 2\chi_0^{\perp} \sigma \left[\chi_{\text{int}}^{(1)} + 3\chi_{\text{int}}^{(3)} x^2 \right], \quad (18)$$

$$\begin{aligned} \chi_{\text{int}}^{(1)} &= 1 - \frac{2}{\sigma} - 2 \left(1 - \frac{3}{\sigma} \right) \frac{\zeta}{\sigma}, \\ \chi_{\text{int}}^{(3)} &= -\frac{4}{3} \left[\left(1 - \frac{3}{\sigma} \right) - \frac{3\zeta}{\sigma} \right]. \end{aligned}$$

Therefore, the final result is the following asymptotic expression for the magnetization taking account of both SA (ζ) and DI ($\tilde{\xi}$), in addition of course to the contributions from the uniaxial anisotropy (σ) and magnetic field (x)

$$m(x, \sigma, \zeta, \tilde{\xi}) \simeq \tilde{\chi}^{(1)} x + \tilde{\chi}^{(3)} x^3 \quad (19)$$

where

$$\tilde{\chi}^{(1)} \simeq \chi_{\text{free}}^{(1)} + \tilde{\xi} \left[1 - \frac{2}{\sigma} - 2 \left(1 - \frac{3}{\sigma} \right) \frac{\zeta}{\sigma} \right], \quad (20)$$

$$\tilde{\chi}^{(3)} \simeq \chi_{\text{free}}^{(3)} - \frac{4}{3} \tilde{\xi} \left[\left(1 - \frac{3}{\sigma} \right) - \frac{3\zeta}{\sigma} \right]$$

are respectively the linear and cubic susceptibilities corrected by DI.

The asymptotic expression (19) shows how SA competes with DI. Indeed, the sign of the surface contribution with intensity ζ plays an important role in the magnetization curve. However, since it appears coupled to the DI $\tilde{\xi}$ parameter, which contains information regarding the sample's shape, it is the overall sign of $\tilde{\xi}\zeta$ that determines whether there is a competition between SE and DI or if the changes in magnetization induced by the intrinsic and collective contributions have concomitant effects. We know that for oblate samples ($\tilde{\xi} < 0$) DI tend to suppress the magnetization, whereas for prolate samples ($\tilde{\xi} > 0$) they enhance it. On the other hand, the effect of SA should be discussed in relation with the quadratic contribution with coefficient K_2 in Eq. (3). Indeed, for $\zeta > 0$ the energy minima of the quartic contribution are along the cube diagonals while for $\zeta < 0$ they are along the cube edges. Hence, the uniaxial anisotropy with an easy axis along the z direction, competes with the cubic anisotropy when $\zeta > 0$ whereas the two anisotropies have a concomitant effect when $\zeta < 0$. Consequently, we see from Eqs. (19, 20) that SE and DI may have opposite or concomitant effects depending on their respective signs. On this basis, and upon plotting the magnetization as a function of the applied field, for different values of ζ , for both prolate and oblate assemblies, a plausible interpretation of the experimental results of Ref. 4, discussed above, was reached in terms of a screening of the

SA effects by DI, assuming that for the studied γ -Fe₂O₃ samples $\zeta > 0$ and $\tilde{\xi} < 0$.

The expression in Eq. (19) for the magnetization of a (weakly) interacting assembly of NM, taking account of surface anisotropy, may be applied to a variety of samples if they can be produced with several concentrations and NM sizes and shapes. In particular, arrays of platelet with varying aspect ratio and separation should provide the necessary conditions for checking these theoretical predictions.

We may obtain the condition under which the SE and DI annihilate each other, at least to first order in x (applied field). Indeed, using Eq. (17) we rewrite Eq. (20) as $\tilde{\chi}^{(1)} = (1 - \frac{1}{\sigma}) + \delta\tilde{\chi}^{(1)}$, where the 1st term is simply the linear susceptibility in the absence of both SE and DI, and $\delta\tilde{\chi}^{(1)}$ the correction

$$\delta\tilde{\chi}^{(1)} \equiv \frac{1}{\sigma} \left(-1 + \frac{2}{\sigma} \right) \zeta + \left(1 - \frac{2}{\sigma} \right) \tilde{\xi} - \frac{2}{\sigma} \left(1 - \frac{3}{\sigma} \right) \zeta \tilde{\xi}.$$

For typical samples one has $1/\sigma \ll 1$ and thereby, at first order the screening condition

$$\lambda_{s.c} \simeq \frac{1}{\mathcal{C}^{(0,0)}} \times \frac{\zeta}{\sigma^2}. \quad (21)$$

Considering the fact that the parameter λ (or ξ) is positive, Eq. (21) implies that a competition between SA and DI can only occur if ζ and $\mathcal{C}^{(0,0)}$ are of the same sign, at all temperatures. This is the case when the ANM has a prolate shape, *i.e.* $\mathcal{C}^{(0,0)} > 0$, and the individual NM have a surface anisotropy that leads (in the ESOP model) to a cubic anisotropy with $\zeta > 0$. Likewise, this competition may also set in for a 2D array of nano-elements for which $\zeta < 0$. Indeed, in this case the (effective) cubic anisotropy has minima along the normal to the array plane whereas the DI drive the magnetization into the plane (since for such an oblate sample $\mathcal{C}^{(0,0)} < 0$). Note also that the condition (21) involves the temperature ($\lambda_{s.c} \propto T^2$) and this to be expected because it is derived from the magnetization which is temperature dependent. In fact, this screening condition shows that for a set of parameters, namely the underlying material (K), the assembly spatial arrangement ($\mathcal{C}^{(0,0)}$), the NM characteristics (V, ζ), there is a compensation between DI and SE due to the underlying processes related with spin fluctuations which are essentially temperature-dependent.

B. AC susceptibility

For the AC susceptibility we need to compute the relaxation rate of the individual NM including both SE and DI, before we can study the competition between the intrinsic features and collective behavior. This was done for monodisperse assemblies in Ref. 32.

For a situation with a longitudinal field, *i.e.* an assembly with anisotropy axes oriented along the field ($\psi = 0$), the transverse response can be considered instantaneous ($\tau_{\perp} = 0$). Hence, with $\tau_{\parallel} = \Gamma^{-1}$ and the equilibrium susceptibility $\chi_{\parallel} = \chi^{\text{eq}}$ given in Eq. (16), the AC susceptibility reads (in the simplest model of Debye)

$$\chi(x, \sigma, \zeta, \tilde{\xi}, \eta) = \frac{\chi_{\parallel}^{\text{eq}}}{1 + i\omega\Gamma^{-1}}. \quad (22)$$

The relaxation rate Γ for a NM with surface effects and interacting within the assembly, was computed in Ref. 32 and will not be reproduced here. Here we only discuss the results obtained there regarding the competition under study. For example, the results in Fig. 5 show that the surface anisotropy, in the case of positive ζ , has the opposite effect compared to DI. This implies that surface effects can screen out the effect of DI or the other way round. This confirms the results of Ref. 28, discussed in the previous section, for equilibrium properties for both negative and positive ζ . We further refer the reader to Ref. 28 where a detailed discussion of the competition between DI and SE was presented in what regards the frequency dependence of the real and imaginary parts of the AC susceptibility and the shift of their respective peaks.

The screening condition here is rather difficult to establish in an analytical form because the relaxation rate, which depends on both ζ and ξ , is only known semi-analytically. Nevertheless, we can establish a screening criterion with regards to the effective temperature θ_{VF} that is very often used in the Vogel-Fulcher law to account for DI. Accordingly, in Ref. 32 we obtained the following analytical expression for θ_{VF}

$$\frac{\theta_{\text{VF}}}{T} = \frac{\zeta}{4} + \frac{1}{6\sigma} (\xi^2 \mathcal{S}) \quad (23)$$

where \mathcal{S} is a function of the superlattice. Obviously, in the absence of DI, and according to our formalism, in the absence of SE as well, θ_{VF} vanishes. However, according to Eq. (23), θ_{VF} may vanish even in the presence of both effects if $\zeta < 0$. Indeed, in this case we obtain the screening condition ($\zeta = -|\zeta|$)

$$\lambda_{s.c} \simeq \sqrt{\frac{3}{2\mathcal{S}}} \times \left(\frac{|\zeta|}{\sigma} \right)^{1/2}. \quad (24)$$

Similarly to the condition (21), derived from the equilibrium magnetization, the present condition involves the assembly superlattice (\mathcal{S}) and the NM parameters (K, V, ζ) and temperature with a different power.

C. Ferromagnetic resonance

Now we come to the last example we would like to discuss ; this is the ferromagnetic resonance (FMR) of

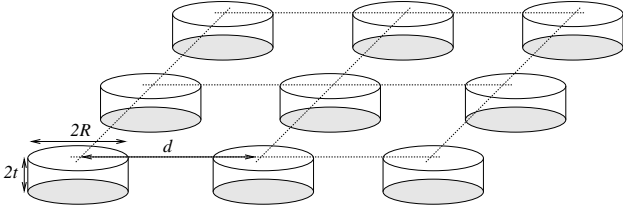


Figure 2: Lattice of thin disks with lattice parameter d .

an interacting ANM. In particular, we investigate the shift of the corresponding frequency induced by SE and DI. In order to derive an approximate expression for the frequency shift due to DI, we consider an array with large enough inter-NM separation so that we can make use of perturbation theory. Then, we split the total energy into a free part plus the interaction contribution [33]

$$\mathbb{H} = \mathcal{F} + \mathcal{I} = \mathcal{F} (1 + \mathcal{F}^{-1} \mathcal{I}).$$

The product $\mathcal{F}^{-1} \mathcal{I}$ scales with the ratio λ/H , *i.e.* the ratio of the DI intensity to the static magnetic field H . This ratio is obviously small for a dilute assembly, especially for standard FMR measurements where the DC field is usually taken strong enough to saturate the sample (usually between 0.3 T and 1 T).

1. Without surface effects

For a 2D array we obtain the explicit DI correction to the FMR (dimensionless) angular frequency ϖ of the array of NM

$$\Delta\varpi_{\text{DI}} \simeq -\frac{\lambda}{2\kappa^3} \times \frac{1}{\mathcal{N}} \sum_{i=1}^{\mathcal{N}} \sum_{j=1, j \neq i}^{\mathcal{N}} \frac{\mathcal{J}_d^h(\eta_{ij}, \tau)}{r_{ij}^3} \quad (25)$$

where $\varpi \equiv \omega/\omega_K$, with $\omega_K \equiv \gamma H_K$, and $\mu_0 H_K = 2K_2/M_s$ the anisotropy field. In addition, we introduce the parameters

$$\kappa \equiv \frac{d}{2R}, \quad \eta_{ij} = \left(\frac{d}{L}\right) r_{ij}.$$

For an array of platelets with $\tau = t/R \ll 1$, as in Fig. 2, the expression above simplifies into

$$\Delta\varpi_{\text{DI}} \simeq \Delta\varpi_{\text{pda}} - \frac{9}{32} \frac{\lambda}{\kappa^5} \mathcal{C}_5 = \Delta\varpi_{\text{pda}} \left(1 + \frac{9}{16\kappa^2} \frac{\mathcal{C}_5}{\mathcal{C}_3}\right) \quad (26)$$

where we have singled out the contribution $\Delta\varpi_{\text{pda}} \equiv -\frac{\lambda}{2\kappa^3} \mathcal{C}_3$ that obtains within the PDA [37], with the usual lattice sums

$$\mathcal{C}_n \equiv \frac{1}{\mathcal{N}} \sum_{i=1}^{\mathcal{N}} \sum_{j=1, j \neq i}^{\mathcal{N}} \frac{1}{r_{ij}^n}.$$

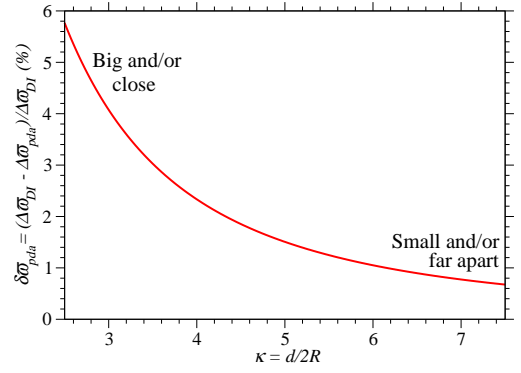


Figure 3: Relative difference between the PDA contribution and that from the finite-size-DI to the FMR frequency.

Several observations may be made. First, we see that while the PDA shift of the resonance frequency behaves, as expected, namely as $1/d^3$, the shift due to finite-size scales as $1/d^5$ for the array of platelets. This contribution is obviously smaller than that of PDA, but it increases as the NM come closer to each other.

Second, as can be seen in Fig. 3, the PDA should be applied only for small and/or well separated NM. To give an order of magnitude we consider the FeV nanodisks studied in Refs. 34, 35 with $2t = 27$ nm, $2R = 600$ nm, $d = 1600$ nm. The results confirm that, for not-too-dense assemblies, *i.e.* for $2.5 \lesssim \kappa \lesssim 3$, there is a variation ($\delta\varpi_{\text{pda}} \simeq 5\%$) of the frequency shift due to the fact that the NM are not simple point dipoles. This variation should be accessible to experiments. Obviously, for very dilute assemblies ($\kappa \gtrsim 7$) the PDA provides a quite reasonable description of the physics up to an error less than 1%.

2. Including surface effects

As was shown in Ref. 33, adding the surface contribution to the free-particle energy according to the effective model (3) adds the term $-\zeta \sum_{\alpha=x,y,z} m_{i,\alpha}^3 \mathbf{e}_\alpha$ to the effective field and thereby the total frequency shift, due to both DI and SE, is given by

$$\Delta\varpi = -\varpi_{\text{SE}} + \Delta\varpi_{\text{DI}} = \zeta - \frac{\lambda}{2\kappa^3} \left[\mathcal{C}_3 + \frac{9}{16\kappa^2} \mathcal{C}_5 \right]. \quad (27)$$

Note that due to the SA contribution, the FMR frequency of a single NM may either increase or decrease according to the sign of ζ . Consequently, for $\zeta > 0$ we see that SA may compete with DI.

Indeed, in Fig. 4 we see that as the NM come closer to each other (smaller κ) the FMR frequency of the interacting array is red-shifted. On the opposite, when ζ becomes positive (going from the black to the blue curve) the FMR frequency is blue-shifted. Second, we see that at some value of ζ and κ , *i.e.* for some parameters of the

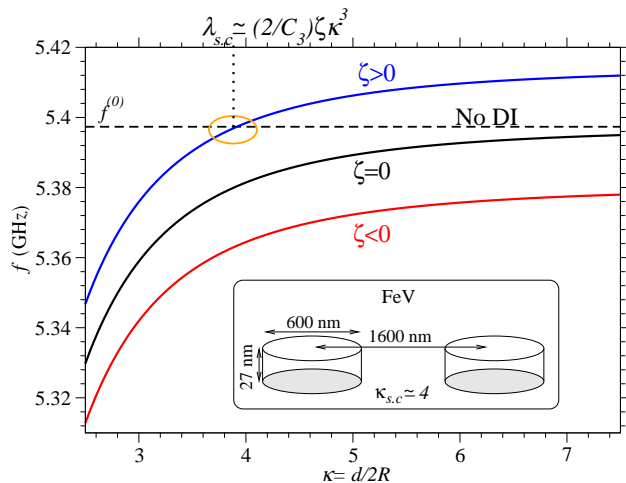


Figure 4: FMR frequency as a function of the NM separation for the noninteracting assembly (dashed line) and for interacting assemblies with $\zeta > 0$ (blue curve), $\zeta = 0$ (black curve), $\zeta < 0$ (red curve).

NM on one hand, and some parameters for the assembly, on the other, the FMR frequency of the interacting array (blue curve) crosses that of the noninteracting assembly (horizontal dashed line). The screening condition in this case is given by

$$\lambda_{s.c.} \simeq \frac{2}{C_3} \times \zeta \kappa^3. \quad (28)$$

Contrary to the conditions (21) and (24), the condition above only depends on the samples properties and not on temperature. This is not surprising knowing that the resonance frequency is an intrinsic property of the sample.

For the FeV disks considered above, we may invert the expression in Eq. (28) to find the numerical condition on κ ; we find $\kappa_{s.c.} \simeq 4$. Such a compensation point could be achieved for some NM assemblies with reasonable physical parameters. For instance, in Ref. 22 it was found that the resonance frequencies of dense assemblies of NiFe nanowires could be recovered using Kittel's expression for noninteracting assemblies [see Fig. 4 of the cited reference]. This means that the DI of the dense assembly are compensated for such nanowires.

V. CONCLUSIONS

After summarizing the theoretical developments that allow us to take into account both the intrinsic and collective effects in an assembly of nanomagnets, we study the competition between surface anisotropy and dipolar interactions through three different observables: the magnetization, the ac susceptibility, and FMR. For each of these observables, we have demonstrated that there ex-

ists a set of physical parameters, pertaining to the nano-elements themselves and to their arrangement in an assembly, for which a compensation between surface effects and inter-element interaction occurs. This implies that the corresponding assembly would behave as noninteracting. In each case, we have given an explicit expression for the screening condition in terms of the physical parameters. The screening conditions in Eqs. (21) and (24) differ significantly from Eq. (28) in the sense that the first two depend on the temperature while the latter does not. This implies that for a specifically synthesized sample the FMR frequency is a more suitable observable for achieving noninteracting assemblies of dressed particles over a large range of temperature. As for the magnetization and ac susceptibility measurements, the temperature scaling laws for the screening condition ($\lambda_{s.c.} \propto T^2$ or $\lambda_{s.c.} \propto T^{1/2}$) imply that one does not need to specifically design a sample in order to have a DI-SA compensation: this situation can be achieved by simply estimating the temperature at which this situation should occur.

Glossary

NM = nanomagnet(s), SNM = single nanomagnet(s), ANM = nanomagnet assembly, SE = surface effects, SA = surface anisotropy, EOSP = effective-one-spin problem, DI = dipolar interaction(s), PDA = point-dipole approximation.

-
- [1] G. J. Strijkers, J. H. J. Dalderop, M. A. A. Broeksteeg, H. J. M. Swagten, and W. J. M. de Jonge, *Journal of Applied Physics* **86**, 5141 (1999), URL <http://scitation.aip.org/content/aip/journal/jap/86/9/10.10>
 - [2] A. Encinas-Oropesa, M. Demand, L. Piraux, U. Ubels and I. Huynen, *J. Appl. Phys.* **89**, 6704 (2001).
 - [3] E. Tronc, D. Fiorani, M. Noguès, A.M. Testa, F. Lucari, F. D'Orazio, J. M. Grenèche, W. Wernsdorfer, N. Galvez, C. Chanéac, D. Mailly, and J. P. Jolivet, *J. Magn. Magn. Mater.* **262**, 6 (2003).
 - [4] E. Tronc, A. Ezzir, R. Cherkaoui, C. Chanéac, M. Noguès, H. Kachkachi, D. Fiorani, A. M. Testa, J. M. Grenèche and J. P. Jolivet, *Surface-related properties of γ -Fe₂O₃ nanoparticles*, *J. Magn. Magn. Mater.* **221**, 63 (2000).
 - [5] D.A. Dimitrov and Wysin, *Effects of surface anisotropy on hysteresis in fine magnetic particles*, *Phys. Rev. B* **50**, 3077 (1994).
 - [6] R.H. Kodama and A.E. Berkovitz, *Atomic-scale magnetic modeling of oxide nanoparticles*, *Phys. Rev. B* **59**, 6321 (1999).
 - [7] H. Kachkachi and D. A. Garanin, *Physica A Statistical Mechanics and its Applications* **300**, 487 (2001), cond-mat/0001278.
 - [8] H. Kachkachi and D. A. Garanin, *European Physical Journal B* **22**, 291 (2001), cond-mat/0012017.

- [9] O. Iglesias and A. Labarta, *Finite-size and surface effects in maghemite nanoparticles: Monte Carlo simulations*, Phys. Rev. B **63**, 184416 (2001).
- [10] H. Kachkachi and M. Dimian, *Hysteretic properties of a magnetic particle with strong surface anisotropy*, Phys. Rev. B **66**, 174419 (2002).
- [11] H. Kachkachi and D.A. Garanin, in *Surface effects in magnetic nanoparticles*, edited by D. Fiorani (Springer, Berlin, 2005), p. 75.
- [12] N. Kazantseva, D. Hinzke, U. Nowak, R. W. Chantrell, U. Atxitia, and O. Chubykalo-Fesenko, *Towards multiscale modeling of magnetic materials: Simulations of FePt*, Phys. Rev. B **77**, 184428 (2008).
- [13] D. A. Garanin and H. Kachkachi, Phys. Rev. Lett. **90**, 065504 (2003), URL <http://link.aps.org/doi/10.1103/PhysRevLett.90.065504>.
- [14] H. Kachkachi, *Effects of spin non-collinearities in magnetic nanoparticles*, J. Magn. Magn. Mater. **316**, 248 (2007).
- [15] D. A. Garanin, Phys. Rev. B **98**, 054427 (2018), URL <https://link.aps.org/doi/10.1103/PhysRevB.98.054427>.
- [16] H. Kachkachi and E. Bonet, *Surface-induced cubic anisotropy in nanomagnets*, Phys. Rev. B **73**, 224402 (2006).
- [17] P.-M. Déjardin, H. Kachkachi, Yu. Kalmykov, *Thermal and surface anisotropy effects on the magnetization reversal of a nanocluster*, J. Phys. D **41**, 134004 (2008).
- [18] W. Wernsdorfer, *Classical and quantum magnetization reversal studied in nanometer-sized particles and clusters*, Adv. Chem. Phys. **118**, 99 (2001).
- [19] M. Jamet, W. Wernsdorfer, C. Thirion, D. Mailly, V. Dupuis, P. Mélinon, and A. Pérez, Phys. Rev. Lett. **86**, 4676 (2001).
- [20] M. Dimian and H. Kachkachi, *Effect of surface anisotropy on the hysteretic properties of a magnetic particle*, J. Appl. Phys. **91**, 7625 (2002).
- [21] P. Vargas and D. Altbir, Phys. Rev. B **62**, 6337 (2000).
- [22] A. F. Franco, J. L. Déjardin, and H. Kachkachi, J. Appl. Phys. **116**, 243905 (2014).
- [23] M. Beleggia, S. Tandon, Y. Zhu, and M. De Graef, J. Magn. Magn. Mater. **278**, 270 (2004).
- [24] A. Ezzir, *Propriétés magnétiques d'une assemblées de nanoparticules: modélisation de l'aimantation et de la susceptibilité superparamagnétique et applications* (Ph.D. thesis, Université Paris-Sud, Orsay, 1998).
- [25] J.P. Chen, C.M. Sorensen, K.J. Klabunde, and G.C. Hadjipanayis, *Enhanced magnetization of nanoscale colloidal cobalt particles*, Phys. Rev. B **51**, 11527 (1995).
- [26] H. Kachkachi, A. Ezzir, M. Noguès, and E. Tronc, *Surface effects in nanoparticles: Monte Carlo simulations*, Eur. Phys. J. B **14**, 681 (2000).
- [27] G. Margaris, K.N. Trohidou, and H. Kachkachi, *Surface effects on the magnetic behavior of nanoparticle assemblies*, Phys. Rev. B **85**, 024419 (2012).
- [28] Z. Sabsabi, F. Vernay, O. Iglesias, H. Kachkachi, *Interplay between surface anisotropy and dipolar interactions in an assembly of nanomagnets*, Phys. Rev. B **88**, 104424 (2013).
- [29] H. Kachkachi and M. Azeggagh, *Magnetization of nanomagnet assemblies: Effects of anisotropy and dipolar interactions*, Eur. Phys. J. B **44**, 299 (2005).
- [30] J.L. Garcia-Palacios, *On the Statics and Dynamics of Magnetoanisotropic Nanoparticles*, Adv. Chem. Phys. **112**, 1 (2000).
- [31] P.E. Jonsson and J.L. Garcia-Palacios, Phys. Rev. B **64**, 174416 (2001).
- [32] F. Vernay, Z. Sabsabi, H. Kachkachi, *ac susceptibility of an assembly of nanomagnets: Combined effects of surface anisotropy and dipolar interactions*, Phys. Rev. B **90**, 094416 (2014).
- [33] J.-L. Déjardin, A. Franco, F. Vernay, and H. Kachkachi, Phys. Rev. B **97**, 224407 (2018), URL <https://link.aps.org/doi/10.1103/PhysRevB.97.224407>.
- [34] K. Mitsuzuka, D. Lacour, M. Hehn, S. Andrieu, and F. Montaigne, Appl. Phys. Lett. **100**, 192406 (2012).
- [35] B. Pigeau et al., Phys. Rev. Lett. **109**, 247602 (2012).
- [36] The anisotropy constant K used in σ is the effective uniaxial anisotropy constant.
- [37] Note that C_3 vanishes for cubes and spheres and for such systems only the first expression in Eq. (26) should be used.